

# Melamine supported on hydroxyapatite-encapsulated- $\gamma$ - $\text{Fe}_2\text{O}_3$ : a novel superparamagnetic recyclable basic nanocatalyst for the synthesis of 1,4-dihydropyridines and polyhydroquinolines

Sedighe Igder · Ali Reza Kiasat ·  
Mohamad Reza Shushizadeh

Received: 9 May 2014 / Accepted: 6 September 2014 / Published online: 1 October 2014  
© Springer Science+Business Media Dordrecht 2014

**Abstract** In this paper, the preparation and characterization of hydroxyapatite-encapsulated  $\gamma$ - $\text{Fe}_2\text{O}_3$  nanoparticles functionalized with Melamine nanocomposite ( $\gamma$ - $\text{Fe}_2\text{O}_3$ @HAp@Melamine) are presented. The resulting nanocomposite was characterized by infrared spectroscopy, scanning electron microscope, thermal gravimetric analysis, X-ray diffraction, vibrating sample magnetometer and elemental analysis. The catalytic activity of  $\gamma$ - $\text{Fe}_2\text{O}_3$ @HAp@Melamine as a magnetic powerful basic nanocatalyst was probed through one-pot synthesis of 1, 4-dihydropyridine and polyhydroquinoline derivatives through Hantzsch condensation reaction under solvent-free thermal conditions. The heterogeneous catalyst could be recovered easily by simple magnetic decantation and reused many times without significant loss of its catalytic activity.

**Keywords** Magnetic basic nanocatalyst · Nano  $\gamma$ - $\text{Fe}_2\text{O}_3$  supported Melamine ·  $\gamma$ - $\text{Fe}_2\text{O}_3$ @HAp · 1,4-Dihydropyridines · Polyhydroquinolines

## Introduction

A long-standing goal in catalysis has been the simple recovery and reuse of highly active homogeneous catalysts via surface grafting to heterogeneous supports [1, 2]. Although the ability of heterogeneous catalysts has been demonstrated successfully in many reactions, the tedious recycle of catalysts via filtration and the inevitable loss of solid catalyst in the separation process limited their application [3–6].

---

S. Igder · A. R. Kiasat (✉)

Chemistry Department, College of Science, ShahidChamran University, 61357-4-3169 Ahvaz, Iran  
e-mail: akiasat@scu.ac.ir

M. R. Shushizadeh

Faculty of Chemistry, Jundishapur University of Medical Sciences, Ahvaz, Iran

Nowadays, to further address the issue of recyclability and reusability, magnetic nanocarriers have been developed. The magnetic nature of these heterogeneous nanocarriers allows for easy recovery and recycling of the catalysts by an external magnetic field, which may optimize operational costs and enhance product purity [7–9].

It is known that iron oxides, magnetite ( $\text{Fe}_3\text{O}_4$ ) and maghemite ( $\gamma\text{-Fe}_2\text{O}_3$ ), are inherently biocompatible and are amenable to post-synthesis surface modification, which makes them excellent candidates for many important applications [10–14]. Although magnetic iron oxide nanoparticles are non-toxic and could be easily synthesized by co-precipitation methods, their applications have been limited due to low chemical and thermal stability in environmental conditions. Thus, the coating of these nanomagnets with an oxygen-impermeable sheath is a necessary prerequisite for their potential use in biomedical and catalyst support applications [15, 16]. Due to good chemical stability, high surface area, and easy synthesis, hydroxyapatite-coated magnetic nanoparticles have recently been introduced and used as a heterogeneous catalytic support [17–19].

On the other hand, heterocyclic compounds embedded with nitrogen are prevalent in nature, and present in numerous natural products and pharmaceutical leads. Among the nitrogen heterocycles, 1, 4-dihydropyridine (DHP) and polyhydroquinoline (PHQ) derivatives exhibit a wide range of notable biological properties which expand their applications as vasodilator, antitumor, bronchodilator, antiatherosclerotic, geroprotective and hepatoprotective agents [20–25]. Moreover, these compounds exhibit several medicinal applications which include neuroprotectant, platelet anti-aggregatory activity, and chemosensitizer acting in tumor therapy [26–31]. Thus, the development of simple synthetic routes for these nitrogen-containing heterocyclic compounds from readily available reagents is an important task in organic synthesis.

The straightforward procedure for this goal, first reported by Arthur Hantzsch in 1882, involves three-component, one-pot cyclocondensation of a  $\beta$ -ketoester with an aldehyde and a nitrogen donor either in acetic acid or in refluxing ethanol [32]. Due to the some limitations of the Hantzsch method for the synthesis of different substituted biologically active DHPs, recently, several methods with improved procedures have been devoted to the preparation of DHP [33–37] and PHQ [38–40]. Although most of these processes offer distinct advantages, they have one or more drawbacks such as unsatisfactory yields, acidic catalysts, prolonged reaction times, tedious work-up, harsh reaction conditions, relatively expensive reagents, environmentally toxic catalysts and the use of large quantities of volatile organic solvents. Consequently, there is scope for further modification towards mild reaction condition, increased variation of the substituents and improved yields.

By considering all the above-mentioned points and recent reports for the application of supported Melamine on the surfaces of nanoparticles [41, 42], the aim of this presented protocol is to highlight the synergistic effects of the combined use of multicomponent reactions, MCRs, and reactions under solvent-free conditions with a heterogeneous magnetic nanocatalyst for the development of new eco-compatible strategy for heterocyclic synthesis. In that regard, we designed, for the first time, hydroxyapatite-encapsulated  $\gamma\text{-Fe}_2\text{O}_3$  nanoparticles functionalized with

Melamine nanocomposite ( $\gamma$ -Fe<sub>2</sub>O<sub>3</sub>@HAp@Melamine) and investigated its performance as a magnetic powerful basic nanocatalyst for the synthesis of DHP and PHQ derivatives through one-pot Hantzsch condensation reaction under solvent-free thermal conditions.

## Experimental

### General remarks

Iron (II) chloride tetrahydrate (99 %), iron (III) chloride hexahydrate (98 %), aldehydes and other chemical materials were purchased from Fluka and Merck and used without further purification. Products were characterized by comparison of their physical data [43–47] and IR and <sup>1</sup>H NMR and <sup>13</sup>C NMR spectra with known samples. NMR spectra were recorded in CDCl<sub>3</sub> on a Bruker Advance DPX 400 MHz instrument spectrometer using TMS as internal standard. The purity determination of the products and reaction monitoring were accomplished by TLC on silica gel polygram SILG/UV 254 plates. The FT-IR spectra of  $\gamma$ -Fe<sub>2</sub>O<sub>3</sub>@HAp and  $\gamma$ -Fe<sub>2</sub>O<sub>3</sub>@HAp@Melamine were measured as potassium bromide discs on a BOMEM MB-Series 1998 FT-IR Spectrophotometer. The particle morphology was examined by SEM. The TGA curve of the nanocomposite was recorded on a BAHR, SPA 503 at heating rates of 10 °C min<sup>-1</sup>. The crystal structure of the nanocomposite was examined using a PW-1840 Philips diffractometer at room temperature utilizing Cu K $\alpha$  radiation wavelength of  $\lambda = 1.5418\text{\AA}$ . The peak position and intensities were obtained between 10° and 80° with a velocity of 0.02° per second. For magnetization measurement, a vibrating sample magnetometer (VSM) (KavirKashanMagnatics, Iran) was used at room temperature.

### Synthesis of HAp-encapsulated- $\gamma$ -Fe<sub>2</sub>O<sub>3</sub>[Fe<sub>2</sub>O<sub>3</sub>@HAp]

Fe<sub>2</sub>O<sub>3</sub>@HAp was synthesized according to the previously reported method [41]. FeCl<sub>2</sub>·4H<sub>2</sub>O (1.85 mmol) and FeCl<sub>3</sub>·6H<sub>2</sub>O (3.7 mmol) were dissolved in deionized water (30 mL) under Ar atmosphere at room temperature and the resulting solution was added to a 25 wt% NH<sub>4</sub>OH solution (10 mL) with vigorous mechanical stirring. A black precipitate of Fe<sub>3</sub>O<sub>4</sub> was produced instantly. In order to obtain small and uniform Fe<sub>3</sub>O<sub>4</sub> particles, the drop rate of NH<sub>4</sub>OH was controlled precisely by a constant dropper and the drop rate was 1 mL min<sup>-1</sup>. After 15 min, 100 mL of Ca(NO<sub>3</sub>)<sub>2</sub>·4H<sub>2</sub>O (33.7 mmol, 0.5 M) and (NH<sub>4</sub>)<sub>2</sub>HPO<sub>4</sub> (20 mmol, 3.0 M) solutions adjusted to pH 11 were added drop-wise to the obtained precipitate over 30 min with mechanical stirring.

The resulting milky solution was heated to 90 °C. After 2 h, the mixture was cooled to room temperature and aged overnight. The dark brown precipitate formed was filtered, washed repeatedly with deionized water until the water was neutral, and then air-dried under vacuum at room temperature. The synthesized sample was calcined at 300 °C for 3 h, giving a reddish-brown powder.

## Synthesis of Melamine supported on hydroxyapatite-encapsulated- $\gamma$ -Fe<sub>2</sub>O<sub>3</sub> [Fe<sub>2</sub>O<sub>3</sub>@HAp@Melamine]

For introducing of isocyanate groups onto the surface of the Fe<sub>2</sub>O<sub>3</sub>@HAp, the core/shell magnetic nanostructure (0.5 g) was dispersed in dry DMF (15 mL) by sonication and then HMDI (1.36 mL, 8.5 mmol) in dry DMF (5 mL) was added drop-wise to the mixture. After mechanically agitation of mixture for 3 h, to graft Melamine onto the surface, Melamine (1.5 g, 8.5 mmol) was dissolved in dry DMF (15 mL) and added drop-wise to the reaction mixture. The mixture was stirred at 70 °C for 3 h. The precipitate was separated by magnetic decantation and washed with CCl<sub>4</sub> several times.

### Basic capacity of $\gamma$ -Fe<sub>2</sub>O<sub>3</sub>@HAp@Melamine

The basic capacity of Fe<sub>2</sub>O<sub>3</sub>@HAp@Melamine was calculated based on titration of the proton-exchanged brine solutions. To an aqueous solution of NaCl (1 M, 0.025 L) with an initial pH 5.9, the Fe<sub>2</sub>O<sub>3</sub>@HAp@Melamine (100 mg) was added and the resulting mixture stirred for 24 h after which the pH of solution increased to 7.29. This is equal to a basic capacity of  $7.01 \times 10^{-6}$  mmol basic sites/g of basic nanocatalyst. Additionally, this result confirmed by back-titration analysis of the catalyst.

### General procedure for the synthesis of 1, 4-dihydropyridine

A mixture of ethyl acetoacetate (0.26 g, 2 mmol), ammonium acetate (0.115 g, 1.5 mmol), aromatic aldehyde (1 mmol), and Fe<sub>2</sub>O<sub>3</sub>@HAp@Melamine (0.15 g) was heated at 80 °C. After satisfactory completion of the reaction and cooling, the reaction mixture was washed with hot ethyl acetate and the catalyst was removed by a magnetic field. The solid residue was isolated and purified by recrystallization in hot EtOH. The formation of products was related by comparing the IR and NMR data with authentic samples and literature data.

### Selected spectral data for the synthesis of 1, 4-dihydropyridine derivatives

Diethyl 4-(4-cyanophenyl)-2,6-dimethyl-1,4-dihydro-3,5-pyridinedicarboxylate: (Table 2-Entry 4) Yield: 90 %; <sup>1</sup>H-NMR(400 MHz, CDCl<sub>3</sub>):  $\delta$  = 1.2 (t, 6 H), 2.5 (s, 6 H), 4.11 (q, 4 H), 5 (s, 1 H), 5.88 (s, 1 H, NH), 7.2–8.3 (m, 4 H). <sup>13</sup>C-NMR (100 MHz, CDCl<sub>3</sub>):  $\delta$  = 13.95, 19.34, 42.12, 60.96, 100.8, 111.9, 117.4, 127.7, 131.1, 139.3, 146.5, 147.50. IR (KBr): 3,360, 2,231.89, 1,698.93, 1,681.04, 1,491.04, 1,212.61, 780 cm<sup>-1</sup>.

Diethyl 4-(4-chlorophenyl)-2,6-dimethyl-1,4-dihydro-3,5-pyridinedicarboxylate: (Table 2-Entry 9) Yield: 93 %; <sup>1</sup>H-NMR(400 MHz, CDCl<sub>3</sub>):  $\delta$  = 1.24 (t, 6 H), 2.33 (s, 6 H), 4.11 (q, 4 H), 4.97 (s, 1 H), 5.88 (s, 1 H, NH), 7.19–7.23 (m, 4 H). <sup>13</sup>C-NMR (100 MHz, CDCl<sub>3</sub>):  $\delta$  = 14.3, 19.6, 39.2, 59.9, 103.8, 127.9, 129.4, 131.7, 144.1, 146.3, 167.5. IR (KBr): 3,360, 1,689, 1,651, 1,487, 1,212, 1,122, 789 cm<sup>-1</sup>.

## General procedure for the synthesis polyhydroquinoline

A mixture of aromatic aldehyde (1 mmol), dimedone (0.14 g, 1 mmol), ethyl acetoacetate (0.13 g, 1 mmol), ammonium acetate (0.115 g, 1.5 mmol), and Fe<sub>2</sub>O<sub>3</sub>@HAP@Melamine (0.15 g) was heated at for 80 °C. Completion of the reactions was monitored by TLC (n-hexan/ethyl acetate 10:3). After satisfactory completion of the reaction and cooling, the reaction mixture was washed with hot ethel acetate and the catalyst was removed by a magnetic field. The solid residue was isolated and purified by recrystallization in hot EtOH.

## Spectral data for the synthesis of PHQ derivatives

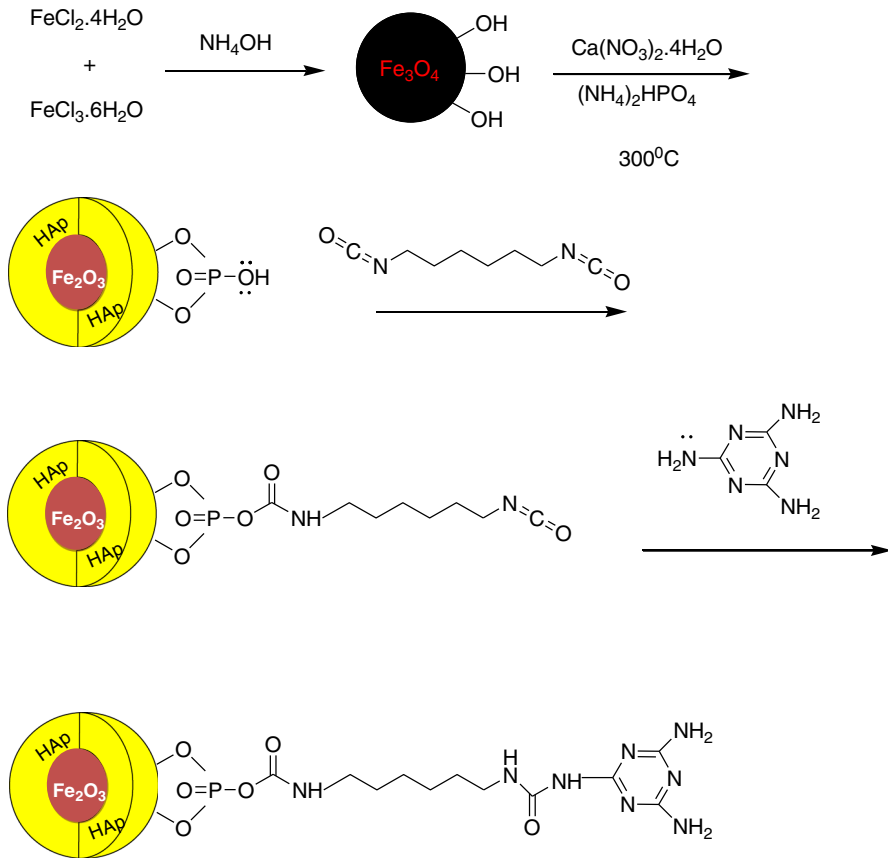
Ethyl 2,7,7-trimethyl-5-oxo-4-(4-chlorophenyl)-1,4,5,6,7,8-hexahydro-3-quinoline-carboxylate (Table 3-Entry 6): Yield: 88 %; M.p 230–232 °C (Ref [42] 233–235 °C); <sup>1</sup>H-NMR (400 MHz, CDCl<sub>3</sub>):  $\delta$  = 1.06 (s, 3H), 1.09 (s, 3H), 1.23 (t, 3H), 2.56 (2H), 2.62(2H), 2.80 (s, 3H), 4.50 (q, 2H), 4.74 (s, 1H), 5.2 (s, 1H), 7.15–7.27 (m, 4H); <sup>13</sup>C-NMR(100 MHz, CDCl<sub>3</sub>):  $\delta$  = 13.95, 16.34, 29.81, 33.31, 38.46, 42.10, 49.81, 60.96, 100.29, 107.65, 127.31, 128.54, 141.22, 142.77, 150.42, 166.49, 196.71. IR (KBr, cm<sup>-1</sup>) 3,273, 3,209, 3,080.51, 2,945, 1,703.89, 1,649.5, 1,475, 1,367, 1,227, 1,105, 857.

Ethyl 2,7,7-trimethyl-5-oxo-4-(4-phenylphenyl)-1,4,5,6,7,8-hexahydro-3-quinoline-carboxylate (Table 3-Entry 11): Yield: 97 %; M.p206–208 °C; <sup>1</sup>H-NMR (400 MHz, CDCl<sub>3</sub>):  $\delta$  = 1.07 (s, 3H), 1.09 (s, 3H), 1.27 (t, 3H), 2.61 (2H), 2.79(2H), 2.95 (s, 3H), 4.50 (q, 2H), 4.91 (s, 1H), 5.7 (s, 1H), 7.2–7.49 (m, 9H); <sup>13</sup>C-NMR(100 MHz, CDCl<sub>3</sub>):  $\delta$  = 13.90, 16.54, 29.88, 33.35, 38.70, 42.20, 49.81, 60.96, 124.68, 126.76, 128.19, 128.84, 139.03, 140.05, 142.77, 144.92, 150.42, 166.49, 196.71. IR (KBr, cm<sup>-1</sup>) 3,302, 3,195, 3,070, 3,218, 1,692, 1,605, 1,475, 1,360, 1,227,1,111, 870.

## Results and discussion

Hydroxyapatite-encapsulated  $\gamma$ -Fe<sub>2</sub>O<sub>3</sub>, Fe<sub>2</sub>O<sub>3</sub>@HAP@Melamine, was synthesized according to the procedure shown in Scheme 1. Maghemitenanocrystallinities are commonly synthesized by coprecipitation of ferrous and ferric ions in a basic aqueous solution followed by thermal treatment. Because of the sensitivity of the  $\gamma$ -Fe<sub>2</sub>O<sub>3</sub>, its surface was first coated with hydroxyapatite [Ca<sub>10</sub>(PO<sub>4</sub>)<sub>6</sub>(OH)<sub>2</sub>, HAp].

Hexamethylenediisocyanate (HMDI), a widely used linker for fabrication of drug delivery vehicles with reportedly a very low degree of toxicity, was used in the present work for conjugating Melamine onto the surface of the  $\gamma$ -Fe<sub>2</sub>O<sub>3</sub>@HAp. For grafting Melamine onto the surface of the  $\gamma$ -Fe<sub>2</sub>O<sub>3</sub>@HAp, the isocyanate groups were preliminarily bonded onto the surface by the reaction of hydroxyl groups of  $\gamma$ -Fe<sub>2</sub>O<sub>3</sub>@HAp with the isocyanate group of HMDI,  $\gamma$ -Fe<sub>2</sub>O<sub>3</sub>@HAp-NCO. After that, the Melamine was reacted with the core/shell magnetic nanostructure.

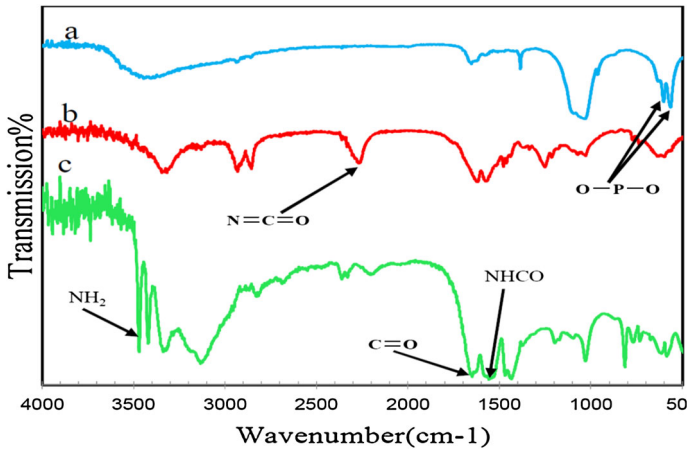


**Scheme 1** Synthesis of  $\gamma\text{-Fe}_2\text{O}_3\text{@HAp@Melamine}$

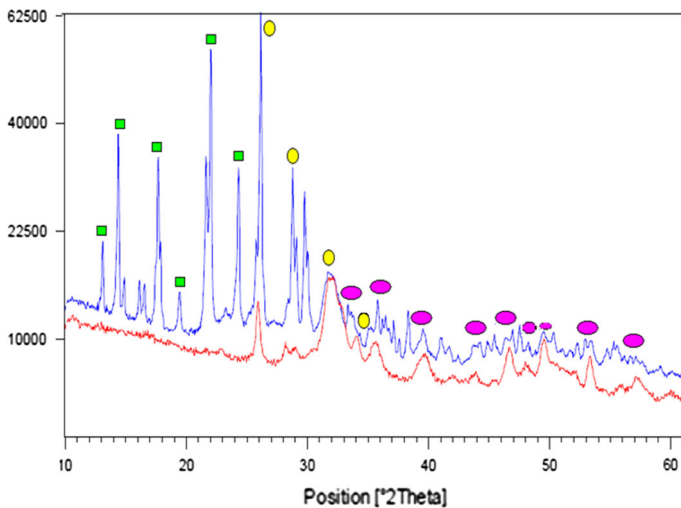
Preparation of  $\gamma\text{-Fe}_2\text{O}_3\text{@HAp@Melamine}$  was confirmed by FT-IR analysis. Figures 1a–c shows the IR spectra of the  $\gamma\text{-Fe}_2\text{O}_3\text{@HAp}$ ,  $\gamma\text{-Fe}_2\text{O}_3\text{@HAp-NCO}$  and  $\gamma\text{-Fe}_2\text{O}_3\text{@HAp@Melamine}$ , respectively. According to the spectra, characteristic absorption bands due to the bending vibration mode of O–P–O surface phosphate groups in the hydroxyapatite shell were observed at  $567$  and  $607\text{ cm}^{-1}$  which overlap with Fe–O stretching.

In addition, the adsorption band at  $1,041\text{ cm}^{-1}$  can be attributed to the stretching of the P–O bond. The IR spectrum of the  $\gamma\text{-Fe}_2\text{O}_3\text{@HAp@Melamine}$  also showed characteristic adsorption bands at  $3,330$  and  $1,630\text{ cm}^{-1}$  corresponding to the NH and C = O groups.

The NHCO stretching was also observed at  $1,570\text{ cm}^{-1}$ . It is worth noting that the disappearance of the isocyanate peak ( $1\text{b}$ ) in the IR spectrum of  $\text{Fe}_2\text{O}_3\text{@HAp@Melamine}$  at about  $2,270\text{ cm}^{-1}$  was also observed. Thus, all the above results indicate that Melamine has been grafted successfully onto the surface of hydroxyapatite-encapsulated  $\gamma\text{-Fe}_2\text{O}_3$  nanoparticles.



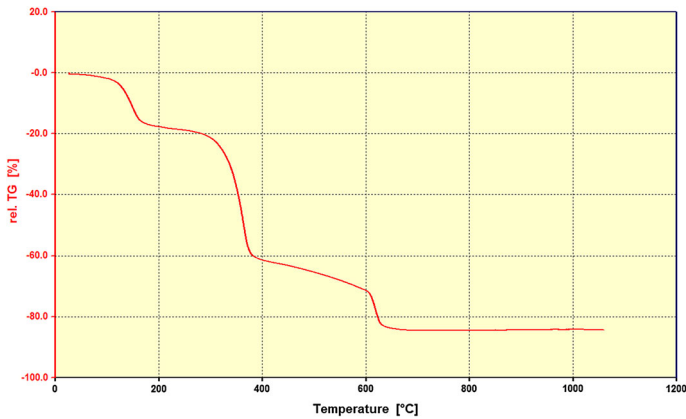
**Fig. 1** The FT-IR spectra of  $\gamma$ - $\text{Fe}_2\text{O}_3$  @HAP (a),  $\gamma$ - $\text{Fe}_2\text{O}_3$  @HAP-NCO (b) and  $\text{Fe}_2\text{O}_3$ @HAP@Melamine (c)



**Fig. 2** XRD spectrum of the  $\gamma$ - $\text{Fe}_2\text{O}_3$ @HAp (red) and  $\gamma$ - $\text{Fe}_2\text{O}_3$ @HAp@Melamine (blue), Yellow circle:  $\gamma$ - $\text{Fe}_2\text{O}_3$ , Pink oval: HAp, Green box: Melamine. (Color figure online)

The  $\gamma$ - $\text{Fe}_2\text{O}_3$ @HAp@Melamine nanocomposite was also characterized by ion exchange pH analysis. The ion-exchange pH analysis demonstrated a loading of  $7.01 \times 10^{-6}$  mmol basic sites  $\text{g}^{-1}$ .

$\gamma$ - $\text{Fe}_2\text{O}_3$ @HAp@Melamine was subject to further structural characterization with XRD (Fig. 2). The peak positions and their relative intensities were determined from a comparison of registered standard JCPDF cards (00-047-1409:  $\gamma$ - $\text{Fe}_2\text{O}_3$ , 00-003-0747: HAp, 00-002-0164: Melamine) available in the system software with the obtained powder diffraction files. The same peaks were observed in both of the bare and Melamine-loaded magnetic particle.



**Fig. 3** The TGA analysis of  $\gamma$ -Fe<sub>2</sub>O<sub>3</sub>@HAp@Melamine

**Table 1** Elemental analysis data of  $\gamma$ -Fe<sub>2</sub>O<sub>3</sub>@HAp@Melamine

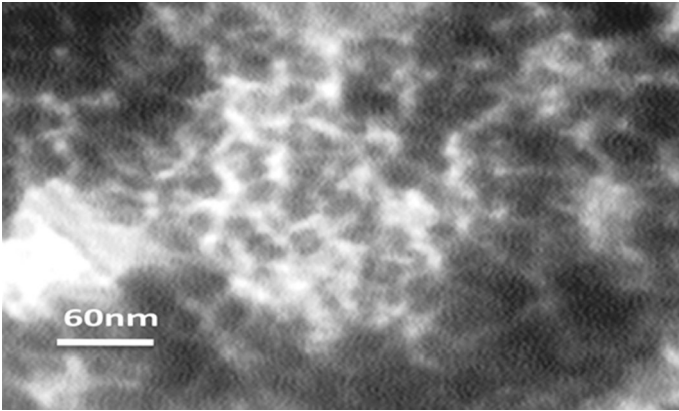
Material	C (W %)	H (W %)	N (W %)
Fe <sub>2</sub> O <sub>3</sub> @HAp@Melamine	27.84	3.83	46.31

Figure 3 shows the TGA analysis of  $\gamma$ -Fe<sub>2</sub>O<sub>3</sub>@HAp@Melamine one can observe from the thermogram that the sample exhibits a three-stage degradation pattern over the range of 30–630 °C. The first weight loss of 16.7 % below 200 °C which might be due to the loss of the adsorbed water as well as dehydration of the surface OH groups. The second weight loss step of about 43.6 % in the region of 310–375 °C was due to the cleavage of the urethane linkage, which is quite high compared to conventional urethanes which generally start to decompose around 200–220 °C. The enhanced thermal stability of  $\gamma$ -Fe<sub>2</sub>O<sub>3</sub>@HAp@Melamine is attributed to its cross-linked nature. The last stage of degradation in the region of 606–637 °C, probably, is due to thermal decomposition of Melamine. Thus, the TGA curves also confirm the successful grafting of Melamine onto the magnetic surface of hydroxyapatite-encapsulated  $\gamma$ -Fe<sub>2</sub>O<sub>3</sub>. The total weight loss over the full temperature range is estimated to be 84.5 % due to the loss of the adsorbed water and organic units. The content of the organic units was also defined by elemental analysis data (Table 1) and is in agreement with thermogravimetric analysis data.

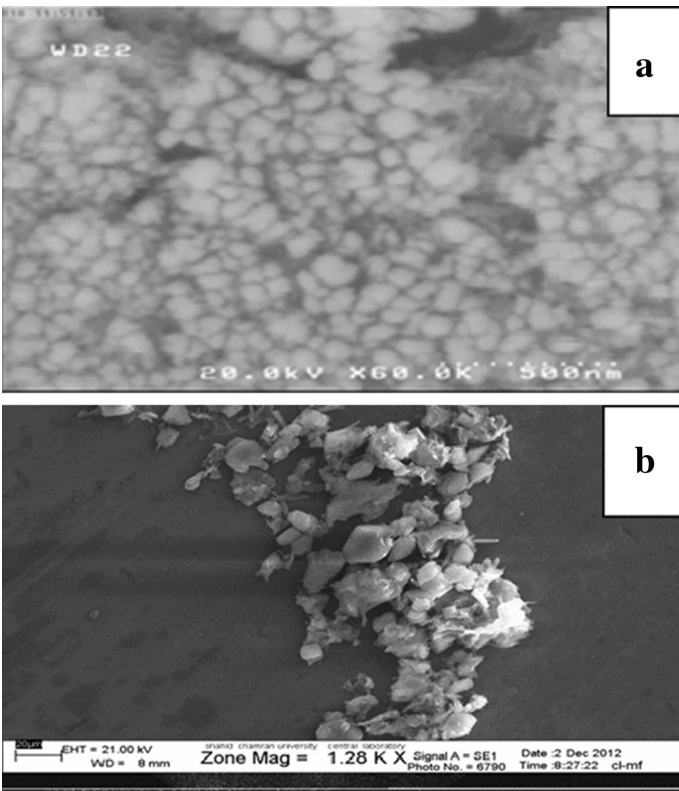
The amount of  $\gamma$ -Fe<sub>2</sub>O<sub>3</sub>@HAp was evaluated by deducting the total weight loss, whose value was obtained from the TGA curve. From these data, the amount of  $\gamma$ -Fe<sub>2</sub>O<sub>3</sub>@HAP is estimated to be 15.5 %.

Atomic absorption spectroscopy (AAS) was also applied to assess the Fe content of the nanocomposite. A GBC (Avanta) Atomic Absorption spectrometer fitted with a Fe hollow cathode lamp (Unicam, Franklin, MA, USA) was used to perform

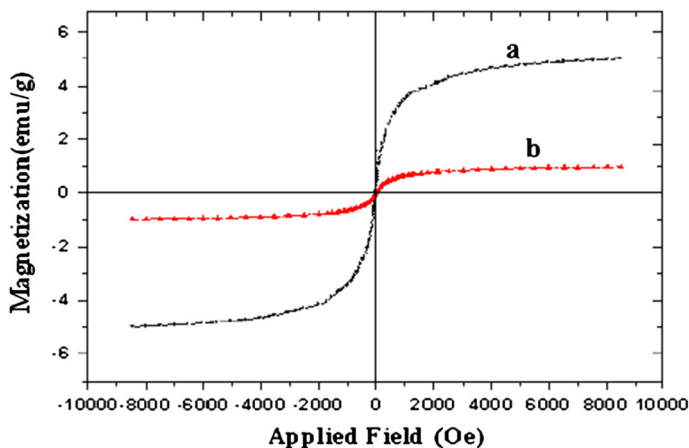




**Fig. 4** TEM image of  $\gamma$ -Fe<sub>2</sub>O<sub>3</sub> @HAp@Melamine



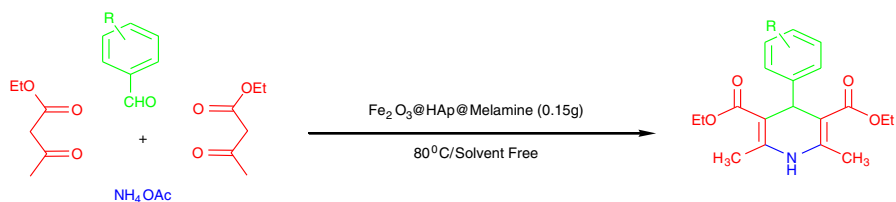
**Fig. 5** SEM images of **a**  $\gamma$ -Fe<sub>2</sub>O<sub>3</sub>@HAp, and **b**  $\gamma$ -Fe<sub>2</sub>O<sub>3</sub>@HAp@Melamine



**Fig. 6** VSM curve of **a**  $\gamma\text{-Fe}_2\text{O}_3$  @HAp and **b**  $\gamma\text{-Fe}_2\text{O}_3$  @HAp@Melamine at room temperature



**Fig. 7** Magnetic recovery of the basic nanocatalyst at the end of reactions



**Scheme 2**  $\gamma\text{-Fe}_2\text{O}_3$  @HAp@Melamine catalyzed synthesis of 1,4-dihydropyridines

atomic absorption measurements. The wavelength of 248.3 nm and spectral bandpass of 0.50 nm were used throughout. An air–acetylene flame was used for the determination of the Fe ions. According to the AAS, the nanocomposite contains 2.5 %  $\text{Fe}_2\text{O}_3$ .

**Table 2** Optimization of the amount of catalyst

Entry	Amount of catalyst (mol %)	Time(min)	Yield(%)
1	0	240	12
2	0.05	40	60
3	0.1	30	79
4	0.15	15	94
5	0.2	15	93

By using the thermogravimetric and AAS data, the empirical formula of the catalyst can be calculated as  $\gamma$ -Fe<sub>2</sub>O<sub>3</sub>(3)@HAp(1)/H<sub>2</sub>O(180)@ C<sub>11</sub>N<sub>8</sub>O<sub>2</sub>H<sub>19</sub>(44.36).

Transmission electron microscopy (TEM) revealed that the iron oxide nanoparticles had been entrapped in the hydroxyapatite shell successfully, in which an average particle size is about 45–60 nm and the diameter of the magnetic core is about 14–29 nm, much smaller than the sizes obtained from the scanning electron microscope (SEM) measurements (Fig. 4).

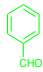
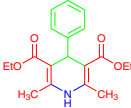
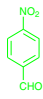
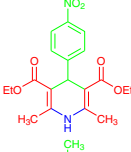
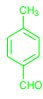
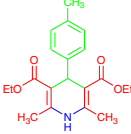
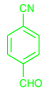
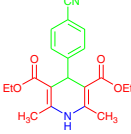
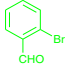
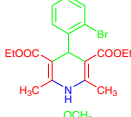

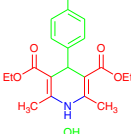
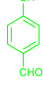
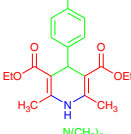
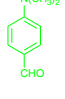
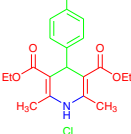
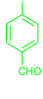
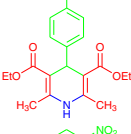
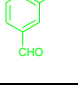
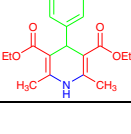
Figure 5 shows SEM photograph of the  $\gamma$ -Fe<sub>2</sub>O<sub>3</sub>@HAp and  $\gamma$ -Fe<sub>2</sub>O<sub>3</sub>@-HAp@Melamine composite particles. This photograph indicates that, although  $\gamma$ -Fe<sub>2</sub>O<sub>3</sub>@HAp particles have a round shape, after grafting Melamine onto its surface by HMDI, the morphology changed.

It is of great importance that the nanocomposite should possess sufficient magnetic and super-paramagnetic properties for its practical applications. As shown in Fig. 6, the isothermal magnetization curves of  $\gamma$ -Fe<sub>2</sub>O<sub>3</sub>@HAp, and  $\gamma$ -Fe<sub>2</sub>O<sub>3</sub>@-HAp@Melamine displayed a rapid increase with increasing applied magnetic field, with a saturation magnetization (M<sub>s</sub>) value of 4.99 and 0.96 emu/g, respectively. Reversibility in the graphs shows that the nanocomposites did not aggregate after the magnet device was removed. The magnetization of the  $\gamma$ -Fe<sub>2</sub>O<sub>3</sub>@HAp@Melamine was also revealed by the easy attraction with an external magnet (Fig. 7).

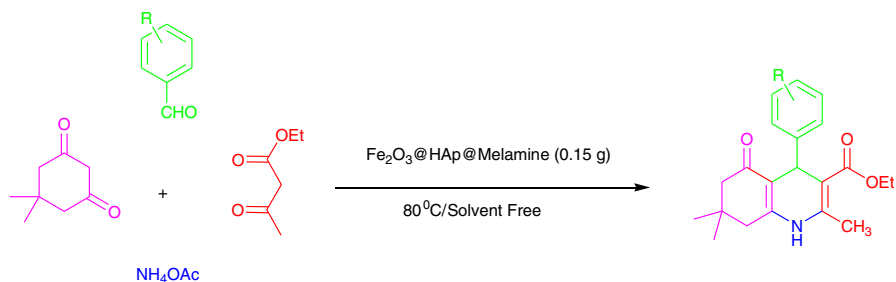
To evaluate the catalytic activity of  $\gamma$ -Fe<sub>2</sub>O<sub>3</sub>@HAp@Melamine as a magnetic powerful basic nanocatalyst and with an aim to develop a simple practical method for the synthesis of a large range of 1,4-dihydropyridines, through multicomponent reaction, initially, three-component coupling reaction of ethyl acetoacetate and benzaldehyde with ammonium acetate in a 2:1:1.5 ratios as a Hantzsch model reaction (Scheme 2) was examined to determine whether the use of  $\gamma$ -Fe<sub>2</sub>O<sub>3</sub>@-HAp@Melamine was efficient and to investigate the optimized conditions.

After some experiments, it was found that for efficient coupling reaction presence of 0.15 g of catalyst under solvent-free conditions at 80 °C is the best condition (15 min, 94 %). Using lower amounts of catalyst, the corresponding DHP was produced in lower yield, while higher amounts of catalyst have no marked effect on the reaction time and yield (Table 2). In order to show the role of the catalyst, a similar reaction in the absence of the catalyst was also examined. Under this

**Table 3** Solvent-free synthesis of 1, 4-dihydropyridine catalyzed by  $\gamma$ -Fe<sub>2</sub>O<sub>3</sub>@HAp@Melamine

Entry	Aldehyde	Product	Time (min)	Yield(%) <sup>a</sup>
1			15	94
2			10	99
3			40	83
4			10	90
5			20	94
6			90	80
7			30	83
8			90	91
9			15	93
10			15	82

<sup>a</sup> Isolated yield



**Scheme 3**  $\gamma$ -Fe<sub>2</sub>O<sub>3</sub>@HAp@Melamine catalyzed synthesis of polyhydroquinoline derivatives

condition, the reaction led to the formation of the desired product in low yield after a long reaction time.

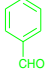
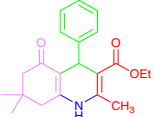
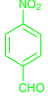
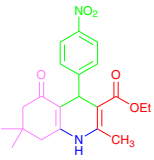
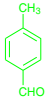
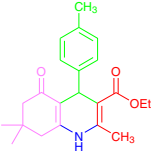
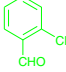
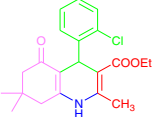
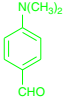
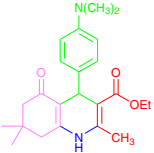
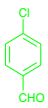
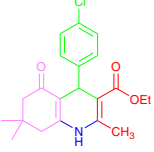
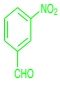
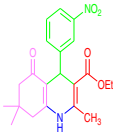
Subsequently, with optimal conditions in hand, 2:1:1.5 molar ratios of ethyl acetoacetate, aldehyde and ammonium acetate and 0.15 g of Fe<sub>2</sub>O<sub>3</sub>@HAp@Melamine at 80 °C under solvent-free conditions, the generality and synthetic scope of this coupling protocol were demonstrated by synthesizing a series of DHPs having different steric and electronic properties. As Table 3 shows, yields are good to excellent in most cases.

With this promising result in hand, to evaluate the generality and synthetic scope of this coupling protocol, a series of PHQ derivatives under the optimized reaction conditions was also prepared through one-pot four-component coupling reaction of ethyl acetoacetate, dimedone and benzaldehyde with ammonium acetate in 1:1:1:1.5 ratios (Scheme 3). The overall process involves the Knoevenagel condensation of dimedone with aryl aldehydes, followed by in situ Michael addition of ethyl acetoacetate in a single operation.

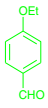
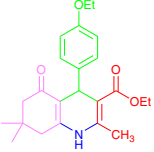
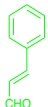
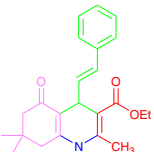
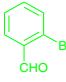
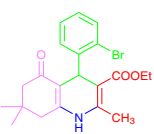
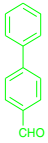
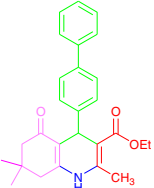
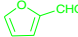
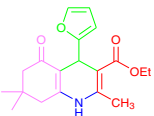
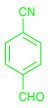
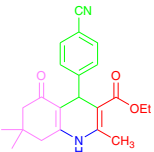
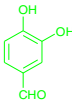
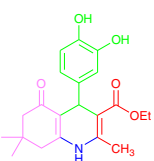
As shown in Table 4, in all cases, heterocyclic, conjugated and aromatic aldehydes with substituents carrying either electron-donating or electron-withdrawing groups reacted successfully and gave the expected products in good to excellent yields and short reaction times. The kind of aldehyde has no significant effect on the reaction. It was indicated that both electron-rich and electron-deficient aldehydes reacted well, mostly leading to high yields of products.

The recyclability of the catalyst in the reaction of benzaldehyde, ethyl acetoacetate, dimedone and ammonium acetate in the presence of  $\gamma$ -Fe<sub>2</sub>O<sub>3</sub>@HAp@Melamine was also checked. After the completion of the reaction, the reaction mixture was cooled to room temperature and hot ethanol was added. The catalyst was concentrated on the sidewall of the reaction vessel using an external magnet, the organic phases were separated by decantation, and the residual catalyst in the reaction vessel was washed and dried and then subjected to the next run directly. In 6 consecutive runs, the conversion stayed higher than 83 %, with no detectable loss (Fig. 8).

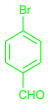
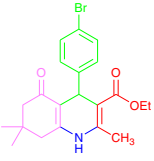
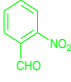
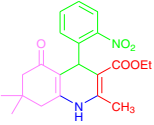
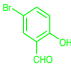
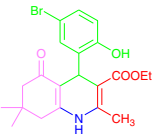
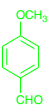
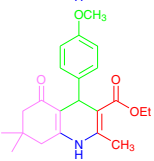
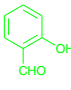
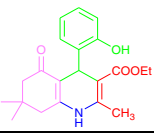
**Table 4** Solvent-free synthesis of polyhydroquinolinecatalyzed by  $\gamma$ -Fe<sub>2</sub>O<sub>3</sub>@HAp@Melamine

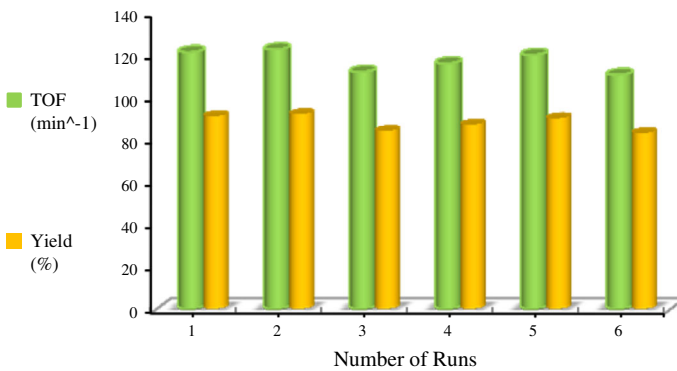
Entry [Ref]	Aldehyde	Product	Time (min)	Yield(%) <sup>a</sup>	M.P. °C	
					Observed	Reported
1			5	89	202–204	203–205 <sup>21</sup>
2			5	91	238–240	242–244 <sup>44</sup>
3			10	89	260–262	260–263 <sup>27</sup>
4			10	89	207–209	207–209 <sup>44</sup>
5			20	95	229–231	233–235 <sup>21</sup>
6			5	88	230–232	233–235 <sup>46</sup>
7			10	85	178–180	172–174 <sup>27</sup>

**Table 4** continued

Entry [Ref]	Aldehyde	Product	Time (min)	Yield(%) <sup>a</sup>	M.P. °C	
					Observed	Reported
8			15	86	oil	–
9			10	87	200–202	203–205 <sup>45</sup>
10			10	95	192–194	NR <sup>b</sup>
11			10	97	206–208	NR <sup>b</sup>
12			30	79	240–242	245–247 <sup>47</sup>
13			10	95	210–213	NR <sup>b</sup>
14			40	72	oil	–

**Table 4** continued

Entry [Ref]	Aldehyde	Product	Time (min)	Yield(%) <sup>a</sup>	M.P. °C	
					Observed	Reported
15			10	82	252–254	252–254 <sup>27</sup>
16			10	85	204–206	204–206 <sup>21</sup>
17			10	81	oil	–
18			10	84	255–257	255–257 <sup>27</sup>
19			15	94	oil	–

<sup>a</sup> Isolated yield**Fig. 8** Recyclability of the  $\gamma$ -Fe<sub>2</sub>O<sub>3</sub>@HAp@Melamin



## Conclusions

In summary, a magnetically separable basic nanocatalyst was successfully prepared through the immobilization of Melamine on hydroxyapatite-encapsulated  $\gamma$ -Fe<sub>2</sub>O<sub>3</sub> nanoparticles. The catalytic activity of  $\gamma$ -Fe<sub>2</sub>O<sub>3</sub>@HAp@Melamine was probed through one-pot synthesis of 1,4-dihydropyridines and PHQ derivatives through Hantzsch condensation reaction under solvent-free thermal conditions. The catalyst shows an environmental friendly character, with recyclability of the catalyst making for the development of a greener strategy. Moreover, the procedure offers several advantages including high yields, operational simplicity, clean reaction conditions and minimum pollution of the environment, which makes it a useful and attractive process for the synthesis of 1,4-dihydropyridines and PHQ derivatives.

**Acknowledgment** We are grateful to the Research Council of ShahidChamran University for financial support.

## References

1. D. Saberi, M. Sheykhani, K. Niknam, A. Heydari, *Catal. Sci. Technol.* **3**, 2025 (2013)
2. M. Gawande, P. Branco, R. Varma, *Chem. Soc. Rev.* **42**, 3371 (2013)
3. S. Wang, Z. Zhang, B. Liu, J. Li, *Catal. Sci. Technol.* **3**, 2104 (2013)
4. S. Sobhani, M. Bazrafshan, A. ArabshahiDelluei, Z. PakdinParizi, *Appl. Catal. A Gen.* **454**, 145–151 (2013)
5. N.E. Leadbeater, M. Marco, *Chem. Rev.* **102**, 3217–3274 (2002)
6. S. Minakata, M. Komatsu, *Chem. Rev.* **109**, 711–724 (2009)
7. L.H. Reddy, J.L. Arias, J. Nicolas, P. Couvreur, *Chem. Rev.* **112**, 5818 (2012)
8. A.R. Kiasat, J. Davarpanah, *J. Mol. Catal. A: Chem.* **373**, 46–54 (2013)
9. B. Atashkar, A. Rostami, B. Tahmasbi, *Catal. Sci. Technol.* **3**, 2140 (2013)
10. M. Gawande, A. Velhinho, I. Nogueira, C.A.A. Ghumman, O.M.N.D. Teodoro, P. Branco, *RSC Adv.* **2**, 6144–6149 (2012)
11. A.R. Kiasat, S. Nazari, *J. Mol. Catal. A: Chem.* **365**, 80–86 (2012)
12. L.A. Mercante, W.W.M. Melo, M. Granada, H.E. Troiani, W.A.A. Macedo, J.D. Ardison, M.G.F. Vaz, M.A. Novak, *J. Magn. Magn. Mater.* **324**, 3029–3033 (2012)
13. N.S. Chaudhari, S.S. Warule, S. Muduli, B.B. Kale, S. Jouen, B. Lefez, B. Hannoyer, S.B. Ogale, *Dalton Trans.* **40**, 8003 (2011)
14. F.B. Li, X.Z. Li, C.S. Liu, T.X. Liu, *J. Hazard. Mater.* **149**, 199–207 (2007)
15. C.H. Woo Lim, I.S. Lee, *Nano Today*, **5**, 412–434 (2010)
16. Y.S. Li, J.S. Church, A.L. Woodhead, *J. Magn. Magn. Mater.* **324**, 1543–1550 (2012)
17. N. Wakiya, M. Yamasaki, T. Adachi, A. Inukai, N. Sakamoto, D. Fu, O. Sakurai, K. Shinozaki, H. Suzuki, *Mater. Sci. Eng. B* **173**, 195–198 (2010)
18. Y. Chengyuan, Z. Yan, C.H. Jing, *Chin J Catal* **32**, 1166–1172 (2011)
19. S.R. Kale, S.S. Kahandal, M.B. Gawande, R.V. Jayaram, *RSC Adv.* **3**, 8184–8192 (2013)
20. S.M. Baghbanian, S. Khaksar, S.M. Vahdat, M. Farhang, M. Tajbakhsh, *Chin. Chem. Lett.* **21**, 563–567 (2010)
21. M. Tajbakhsh, H. Alinezhad, M. Norouzi, S. Baghery, M. Akbari, *J. Mol. Liq.* **177**, 44–48 (2013)
22. A. Rajack, K. Yuvarajua, Ch. Praveena, Y.L.N. Murthy, *J. Mol. Catal. A Chem.* **370**, 197–204 (2013)
23. F. Tamaddon, S. Moradi, *J. Mol. Catal. A Chem.* **370**, 117–122 (2013)
24. A. Sausins, G. Duburs, *Heterocycles* **7**, 269 (1988)
25. J. Safari, S.H. Banitaba, S.D. Khalili, *J. Mol. Catal. A Chemical.* **335**, 46–50 (2011)
26. L.M. Wang, J. Sheng, L. Zhang, J.W. Han, ZhY Fan, H. Tian, C.T. Qian, *Tetrahedron* **61**, 1539–1543 (2005)
27. A. Khojastehnezhad, F. Moeinpour, A. Davoodnia, *Chin. Chem. Lett.* **22**, 807–810 (2011)
28. J. Li, P. He, C. Yu, *Tetrahedron* **68**, 4138–4144 (2012)

29. L. Saikia, D. Dutta, D.K. Dutta, *Catal. Commun.* **19**, 1–4 (2012)
30. M. Saha, A.K. Pal, *Tetrahedron Lett* **52**, 4872–4877 (2011)
31. S. Phukan, M. Saha, A.K. Pal, S. Mitra, *J. Mol. Struct.* **1039**, 119–129 (2013)
32. A. Hantzsch, *Ann. Chem.* **1**, 215 (1882)
33. A. Heydari, S. Khaksar, M. Tajbakhsh, H.R. Bijanzade, *J. Fluorine Chem.* **130**, 609–614 (2009)
34. H. Khabazzadeh, I. Sheikhshoae, S. Saeid-Nia, *Trans. Met. Chem.* **35**, 125–127 (2010)
35. N. Koukabi, E. Kolvari, M.A. Zolfigol, *Adv. Synth. Catal.* (2012). doi:[10.1002/adsc.201100352](https://doi.org/10.1002/adsc.201100352)
36. P.P. Ghosh, S. Paul, A.R. Das, *Tetrahedron Lett.* **54**, 138–142 (2013)
37. S. Balalaie, L. Baoosi, F. Tahoori, F. Rominger, H.R. Bijanzadeh, *Tetrahedron* **69**, 738–743 (2013)
38. R. Surasani, D. Kalita, A.V. DhanunjayaRao, K. Yarbagi, K.B. Chandrasekhae, *J. Fluor. Chem.* **135**, 91–96 (2012)
39. N.K. Ladani, D.C. Mungra, M.P. Patel, R.G. Patel, *Chin. Chem. Lett.* **22**, 1407–1410 (2011)
40. M. Hong, C. Cai, W.B. Yi, *J. Fluor. Chem.* **131**, 111–114 (2010)
41. R.P. Modi, V.N. Mehta, S.K. Kailasa, *Sens. Actuators B* **195**, 562 (2014)
42. S.K. Kailasa, H.F. Wu, *J. Indust, Eng. Chem.* (2014). doi:[10.1016/j.jiec.2014.03.012](https://doi.org/10.1016/j.jiec.2014.03.012)
43. Y. Chengyuan, Z. Yan, C. Jing, *Chin. J. Cata.* **32**, 1166 (2011)
44. M. Tajbakhsh, E. Alae, H. Alinezhad, M. Khanian, F. Jahani et al., *Chin. J. Catal.* **33**, 1517–1522 (2012)
45. G. Sabitha, G.S.K. Reddy, C.S. Reddy, J.S. Yadav, *Tetrahedron Lett.* **44**, 4129 (2003)
46. M.M. Heravi, K. Bakhtiari, N.M. Javadi, F.F. Bamoharram, M. Saeedi, H.A. Oskooie, *J. Mol. Catal. A Chem.* **264**, 50 (2007)
47. J.G. Brietenbucher, G. Figliozzi, *Tetrahedron Lett.* **41**, 4311 (2000)